Series Resistance Compensation for Whole-Cell Patch-Clamp Studies Using a Membrane State Estimator

Adam J. Sherman, Alvin Shrier, and Ellis Cooper
Department of Physiology, McGill University, Montréal, Québec, Canada

ABSTRACT   Whole-cell patch-clamp techniques are widely used to measure membrane currents from isolated cells. While suitable for a broad range of ionic currents, the series resistance (R_s) of the recording pipette limits the bandwidth of the whole-cell configuration, making it difficult to measure rapid ionic currents. To increase bandwidth, it is necessary to compensate for R_s. Most methods of R_s compensation become unstable at high bandwidth, making them hard to use. We describe a novel method of R_s compensation that overcomes the stability limitations of standard designs. This method uses a state estimator, implemented with analog computation, to compute the membrane potential, V_m, which is then used in a feedback loop to implement a voltage clamp; we refer to this as state estimator R_s compensation. To demonstrate the utility of this approach, we built an amplifier incorporating state estimator R_s compensation. In benchtop tests, our amplifier showed significantly higher bandwidths and improved stability when compared with a commercially available amplifier. We demonstrated that state estimator R_s compensation works well in practice by recording voltage-gated Na^+ currents under voltage-clamp conditions from dissociated neonatal rat sympathetic neurons. We conclude that state estimator R_s compensation should make it easier to measure large rapid ionic currents with whole-cell patch-clamp techniques.

INTRODUCTION

Most electrophysiological studies designed to measure ionic currents from single cells use whole-cell patch-clamp techniques. While these techniques are suitable for a broad range of ionic currents, the limited bandwidth of the whole-cell configuration makes it difficult to measure rapid ionic currents, such as voltage-gated Na^+ currents from nerve or muscle cells. The major factor that limits the voltage clamping bandwidth in the whole-cell configuration is the series resistance (R_s) introduced by the recording pipette (Sigworth, 1983). Therefore, to measure rapidly activating currents reliably, it is necessary to increase the voltage clamping bandwidth by compensating for R_s. The main difficulty with commonly used R_s compensation techniques is the instability that arises at high voltage clamping bandwidth. This instability makes measurements of rapid ionic currents with the whole-cell patch-clamp configuration extremely difficult.

To overcome the problem of instability, we have developed a novel approach to R_s compensation that is based on a membrane state estimator. State estimator R_s compensation overcomes the stability limitations of standard designs and is simple and straightforward to use. In this paper, we outline the theory of state estimator R_s compensation. Next, we demonstrate the high bandwidth and stable performance of state estimator R_s compensation and compare it with various methods currently in use to compensate for R_s. Finally, we show the utility of state estimator R_s compen-

sation by measuring voltage-gated Na^+ currents from dissociated neonatal rat sympathetic neurons. Our results clearly illustrate the advantages of state estimator R_s compensation for measuring rapidly activating ionic currents in single cells.

THEORY

Voltage clamping bandwidth and standard R_s compensation

The time constant that determines the whole-cell voltage-clamp bandwidth is given by $\tau_{vclamp} \approx R_s C_m$ when $R_m \gg R_s$, where R_m is the cell membrane resistance and C_m is the cell membrane capacitance (Sigworth, 1983). With typical values for R_s and C_m (5–20 MΩ; 15–100 pF), τ_{vclamp} is several hundred microseconds; this is too slow to voltage clamp rapid ionic currents.

The standard method for compensating for R_s and increasing bandwidth is to compute a scaled value of the pipette current (I_p) and add it as a correction signal to the command potential (V_c) (see Fig. 1). Ideally, when the scaling factor α approaches unity, corresponding to 100% R_s compensation, the membrane potential (V_m) follows V_c exactly. In practice, when α is greater than ~0.8, standard R_s compensation becomes unstable. For wide bandwidth R_s compensation, the instability results from two main factors: 1) limited bandwidth in the current-measuring circuitry and 2) the effects of stray pipette capacitance (C_p) (Sigworth, 1983; also see the Appendix). For stability at 90% R_s compensation, the bandwidth of the current measurement circuitry that generates the R_s correction signal must be greater than 300 kHz, which is difficult to achieve in practice. More importantly, C_p introduces an erroneous correction signal not modeled in Fig. 1 that destabilizes the R_s
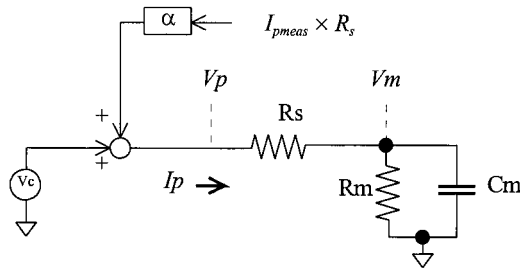
FIGURE 1 Standard R_s compensation for a single electrode voltage clamp: $V_p = V_c + \alpha I_{pmeas}R_s$, $V_m = V_p - I_pR_s$ ∴ $V_m = V_c$ if $I_{pmeas} = I_p$ and $\alpha \rightarrow 1$. V_c = command voltage, V_p = pipette voltage, V_m = membrane voltage, I_p = pipette current, R_s = pipette series resistance, R_m = cell resistance, C_m = cell capacitance.

compensation feedback loop. For stable operation, C_p must be neutralized electronically to <0.05 pF (Sigworth, 1983); slight shifts in pipette capacitance, as happen when the pipette immersion depth changes, easily drive the R_s compensation circuitry from a marginally stable state into oscillation. Consequently, it is exceedingly difficult to achieve the wide bandwidth and stability necessary to measure rapidly activating currents with amplifiers that incorporate standard R_s compensation.

The two-electrode configuration and the membrane voltage estimator

A successful approach to overcoming the effects of R_s is to use two electrodes instead of one. A two-electrode voltage clamp uses one electrode to measure V_m and the other electrode to pass current; V_m is clamped at V_c with a

negative feedback loop (see Fig. 2 A). In this arrangement, R_s is contained within the feedback loop and produces little limitation on the voltage clamp bandwidth because its effects are attenuated by the large open-loop gain of the feedback circuit.

Our approach to R_s compensation for a single-electrode voltage clamp is based on the two-electrode topology in conjunction with a membrane state estimator, as shown in Fig. 2 B. The state estimator computes V_m and functions as a "virtual electrode" in place of the physical measuring electrode and voltage follower. We call this configuration state estimator R_s compensation.

Using only a single electrode, state estimator R_s compensation achieves a bandwidth and stability similar to those of a two-electrode voltage-clamp amplifier. The closed-loop bandwidth and steady-state error become independent of R_s, effectively achieving 100% R_s compensation. Stability is greatly improved over standard R_s compensation by eliminating the need to neutralize C_p electronically. Equally important, state estimator R_s compensation is independent of cell conductance changes, ensuring wide voltage-clamp bandwidth, even during the measurements of large ionic currents.

State estimator theory

The recording patch pipette electrode can be modeled as in Fig. 3. Given that I_p, V_p, R_s, and C_p are known values as defined in Fig. 3, V_m can be estimated as follows:

Applying Kirchoff's current law gives

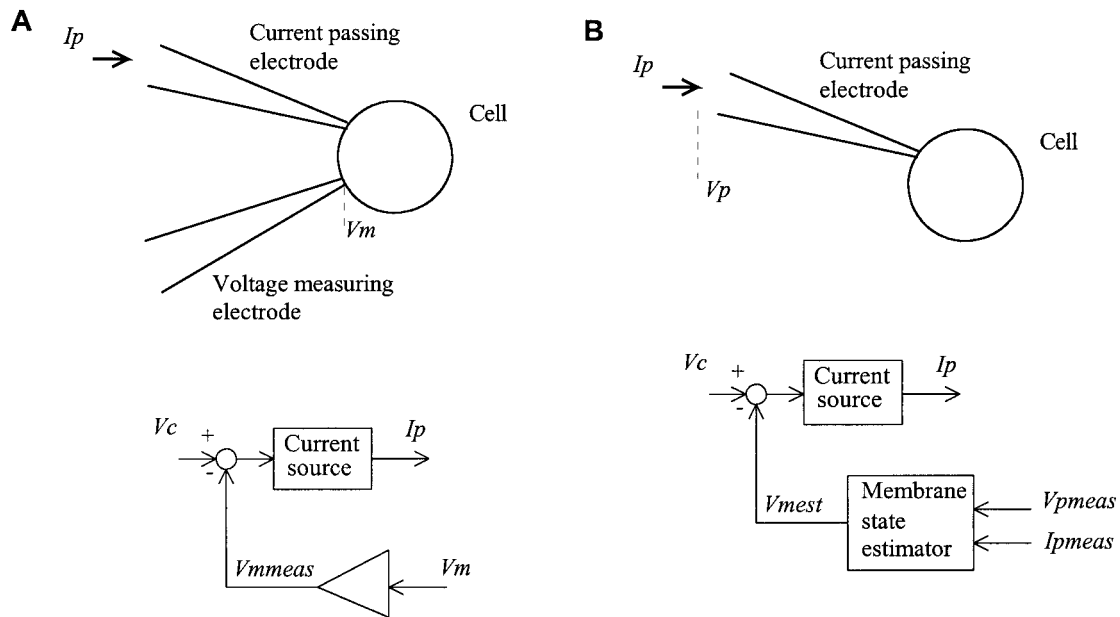$$I_{pr} = I_p - I_{pc} \tag{1}$$

FIGURE 2   (A) Two-electrode voltage clamp. (B) Single-electrode voltage clamp using a membrane state estimator. V_c = command voltage, V_p = pipette voltage, V_m = membrane voltage, I_p = pipette current, I_{pmeas} = measured pipette current, V_{pmeas} = measured pipette voltage, V_{mmeas} = measured membrane voltage, V_{mest} = estimated membrane voltage.
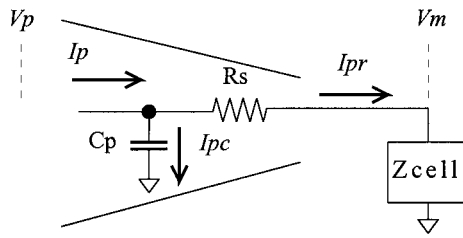
FIGURE 3   Lumped parameter RC model of patch pipette: V_p = pipette voltage, V_m = cell voltage, I_p = total pipette current, I_{pc} = pipette capacitive current, I_{pr} = pipette resistive current, R_s = pipette series resistance, C_p = pipette capacitance, Z_{cell} = cell impedance.

Applying Ohm's law gives

$$V_m = V_p - I_{pr}R_s \tag{2}$$

Substituting Eq. 1 into Eq. 2 gives

$$V_m = V_p - (I_p - I_{pc})R_s \tag{3}$$

From generalized Ohm's law,

$$I_{pc} = V_pC_ps \tag{4}$$

Substituting Eq. 4 into Eq. 3 gives

$$V_m = (\tau_ps + 1)V_p - I_pR_s \tag{5}$$

where τ_p = pipette time constant = R_sC_p and s is the Laplace transform frequency variable. Once R_s and C_p are determined for the patch pipette electrode, Eq. 5 can be solved in real time to compute V_m independently of cell conductance changes.

Bandwidth and stability of state estimator R_s compensation

Fig. 4 A shows the block diagram for a single-electrode voltage clamp incorporating state estimator R_s compensation. In Fig. 4 A, block 1 represents a controlled current source, with gain G_0 in units of conductance and bandwidth set by τ_{cs}. Block 2 gives the transfer function of pipette voltage to pipette current when the pipette is modeled as in Fig. 3 and the cell is modeled as in Fig. 1. Blocks 3, 4, and 5 implement Eq. 5, with τ_{Vpmeas} setting the pipette voltage measurement bandwidth, τ_{Ipmeas} setting the pipette current measurement bandwidth, and τ_{vest} setting the state estimator output bandwidth. Full R_s compensation occurs when R_{sest} in block 3 is set equal to R_s and τ_{pest} in block 4 is set equal to the pipette time constant τ_p.

Fig. 4, B and C, shows the typical performance of state estimator R_s compensation in the frequency domain (Fig. 4 B) and the time domain (Fig. 4 C), using representative parameter values. The Bode plot in Fig. 4 B shows a gain margin of 17 dB and a phase margin of 62°, ensuring stable voltage clamping with full R_s compensation. The closed-loop voltage-clamping bandwidth is roughly equal to the open-loop 0-dB cross-over frequency (10 kHz). This 10-

kHz bandwidth translates to a step response time of less than 50 μs, as shown in Fig. 4 C. These wide stability margins ensure stable performance even if parameters shift during an experiment. (A comparative stability analysis is given in the Appendix.)

To achieve the stability margins in Fig. 4, state estimator R_s compensation requires close phase matching of the I_p and V_p signals up to ~50 kHz. In contrast, obtaining similar stability margins with standard R_s compensation requires bandwidths greater than 300 kHz (Sigworth, 1983); such bandwidths are difficult to achieve in practice. In addition, standard R_s compensation requires near-perfect C_p nulling, whereas C_p nulling is not needed with state estimator R_s compensation. However, as with standard R_s compensation, the value of C_p, once determined, must not fluctuate for stability to be maintained.

Other approaches for R_s compensation

Moore et al. (1984) and Strickholm (1995b) each describe modifications to standard R_s compensation that feed back a scaled value of the steady-state pipette current as opposed to the total pipette current. The steady-state current is computed using an electronic bridge that subtracts the transient membrane capacitive current from the measured total pipette current. While this approach can achieve 100% R_s compensation in the steady state, it is not suitable for measurements during large, rapid (<1 ms) changes in membrane conductance.

Because the bridge is balanced only for a fixed value of R_m, large changes in membrane conductance will unbalance the bridge and voltage control returns slowly. As shown in Fig. 5 A, with typical pipette and cell parameters and a step conductance change from 2 to 50 nS, the voltage recovers in ~1 ms; this is too slow to voltage clamp fast ionic currents. Adding a "supercharging" potential to V_c speeds voltage-clamp control for a step change in V_c (Strickholm, 1995a) but does not improve the voltage recovery time when the membrane conductance changes (compare *dotted and solid lines* in Fig. 5 A). In contrast, state estimator R_s compensation is independent of cell conductance changes, ensuring rapid voltage-clamp recovery from changes in ionic conductance as well as changes in V_c, as shown in Fig. 5 B.

Brennecke and Lindemann (1972) described another approach to overcoming R_s (see also Wilson and Goldner, 1975). Variously called switch-clamp, pulsed current clamp, or discontinuous feedback voltage-clamp amplifiers, these designs operate by repetitively cycling a single electrode between current-passing and voltage-measuring modes. During voltage-measuring mode the amplifier passes no current, ensuring that the measured voltage reflects V_m independently of R_s. The attainable bandwidth is limited by the maximum switching rate, yet this switching rate is itself limited by C_p (Finkel and Redman, 1984). Consequently, to increase bandwidth it is necessary to neutralize C_p electronically, as with standard R_s compensation.
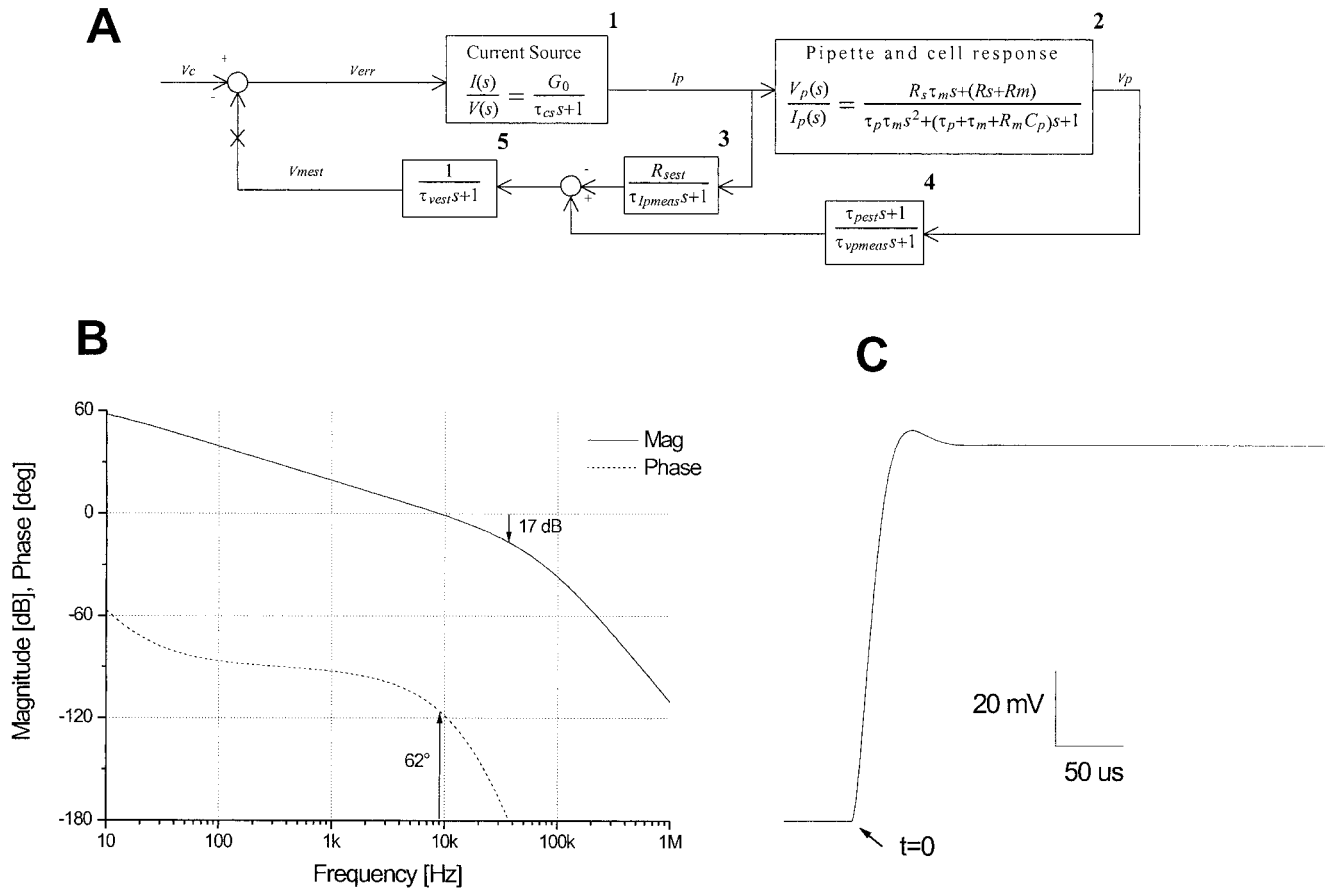
A

B

C

FIGURE 4   Stability of state estimator R_s compensation. (*A*) s-domain block diagram of single-electrode voltage clamp using state estimator R_s compensation. (*B*) Open-loop Bode plot of V_{mest} $(s)/V_c$ (s), where $s = j2\pi f$, with the feedback path broken at *X*. (*C*) Closed-loop step response plot of V_m when V_c undergoes a stepwise transition from 0 to 100 mV at $t = 0$. $R_s = 5$ MΩ, $C_p = 1$ pF, $R_m = 500$ MΩ, $C_m = 50$ pF, τ_{Vpmeas}, τ_{Ipmeas}, $\tau_{vmest} = 1.6$ μs, $\tau_{cs} = 0.32$ μs, $G_0 = 3$ μA/V. V_c = command voltage, V_{err} = error voltage, I_p = pipette current, V_p = pipette voltage, V_{mest} = computed membrane voltage, $\tau_p = R_s C_p$ = pipette time constant, $\tau_m = R_m C_m$ = membrane time constant, τ_{cs} sets current source bandwidth, τ_{Ipmeas} sets I_p measurement bandwidth, τ_{Vpmeas} sets V_p measurement bandwidth, τ_{vest} sets membrane state estimator bandwidth.

This C_p neutralization compromises the stability of the voltage clamp. The attainable voltage-clamp bandwidth using discontinuous feedback is generally insufficient to measure rapidly activating currents, such as voltage-gated Na$^+$ currents from nerve or muscle.

MATERIALS AND METHODS

Amplifier benchmarks

We built a voltage-clamp amplifier implementing the state estimator R_s compensation described in the Theory section and tested its performance using the model membrane and the low-noise dynamic switch shown in Fig. 6. This single-pole single-throw (SPST) switch makes a clean, single-step transition with no detectable switching artifact. We constructed this switch by attaching two silver chlorided wires separated by ~1 cm to the inside of a microcentrifuge tube with a small hole drilled in the bottom. A dilute salt solution established the electrical contact; when the fluid drained from the tube the contact was broken (see Fig. 6). With the switch initially open, we adjusted the amplifier for full R_s compensation by giving repetitive voltage test pulses and adjusting R_{sest} and τ_{pest} (see Fig. 4) to minimize the capacity current transient decay time. The current source gain (G_o, Fig. 4) was then increased to 10 μA/V. The microcentrifuge tube was then filled with salt solution, and the current monitor output of the amplifier was

captured using a Nicolet model 3091 digital oscilloscope (Nicolet Instrument Corporation, Madison, WI) when the switch made the closed to open state transition. As a comparison we repeated the test using an Axopatch 1D with standard R_s compensation (Axon Instruments, Foster City, CA).

Electrophysiological recordings

We made whole-cell patch-clamp recordings from neonatal rat superior cervical ganglia (SCG) neurons. Neonatal rat SCG neurons were cultured for 12–72 h as described by McFarlane and Cooper (1992). All experiments were done at 23°C, using the following solutions (in mM): Pipette solution: 50 KAc, 65 KF, 5 NaCl, 0.2 CaCl$_2$, 1 MgCl$_2$, 10 HEPES, 10 EGTA. (In some experiments K$^+$ currents were blocked by replacing K$^+$ with Cs$^+$.) Extracellular solution: 140 NaCl, 5.4 KCl, 0.3 NaH$_2$PO$_4$, 0.44 KH$_2$PO$_4$, 2.8 CaCl$_2$, 0.18 MgCl$_2$, 10 HEPES, 5.6 glucose. Electrodes were made with a two-stage micropipette puller (model PP-83; Narishige Instrument Co., Tokyo, Japan) from Kimax-51 glass capillary tubes (Kimble Science Products, Chicago, IL). Resistance measured in the bath was 2–5 MΩ; whole-cell access resistance was 3–13 MΩ. In some experiments, the electrodes were coated with Sylgard (Dow Corning, Auburn, MI). Once in whole-cell mode, we obtained full R_s compensation by giving hyperpolarizing test pulses and adjusting R_{sest} and τ_{pest} (see Fig. 4) to minimize the capacity current transient decay time. Then we increased the current source gain (G_o, Fig. 4) to achieve a closed-loop bandwidth greater than 10 kHz.
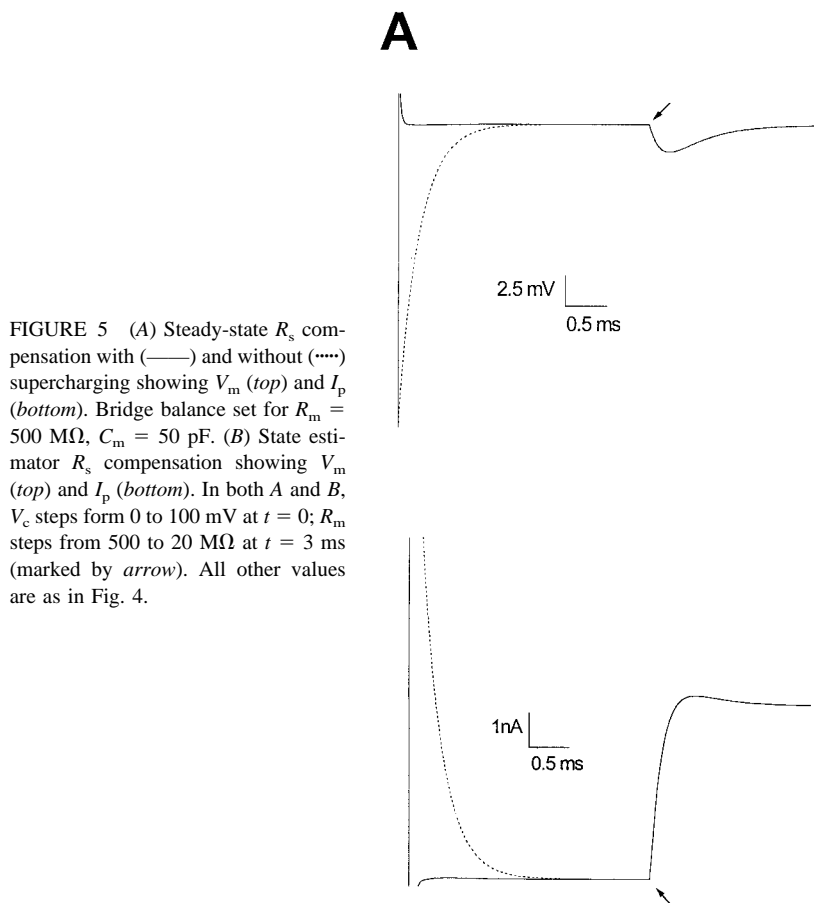
A

B

FIGURE 5   (*A*) Steady-state R_s compensation with (——) and without (·····) supercharging showing V_m (*top*) and I_p (*bottom*). Bridge balance set for $R_m =$ 500 MΩ, $C_m = 50$ pF. (*B*) State estimator R_s compensation showing V_m (*top*) and I_p (*bottom*). In both *A* and *B*, V_c steps form 0 to 100 mV at $t = 0$; R_m steps from 500 to 20 MΩ at $t = 3$ ms (marked by *arrow*). All other values are as in Fig. 4.

2.5 mV

0.5 ms

2.5 mV

0.5 ms

1nA

0.5 ms

1nA

0.5 ms

In all cases, G_o was greater than 5 μA/V, and the capacity current transient decay time was less than 70 μs. This tuning procedure took ~20 s. PatchKit software (Alembic Software, Montréal, Québec, Canada) was used for simultaneous on-line stimulation and acquisition. Voltage-clamp recordings were low-pass filtered at 15 kHz with a single-pole RC filter and digitized at 100 kHz with an IBM-compatible 33-MHz 486 computer equipped with a DAS-20 acquisition board (Omega Engineering, Stamford, CT).

RESULTS AND DISCUSSION

Amplifier benchmarks

To demonstrate the value of state estimator R_s compensation, we built a prototype single-electrode voltage-clamp amplifier that incorporated state estimator R_s compensation as described in the Theory section and compared its performance to a commercial amplifier with standard R_s compensation (Axopatch 1D). To test the performance of both amplifiers, we measured their responses to a step change in conductance. While it would have been simpler to test the performance using a fixed-conductance model membrane, such tests can be misleading when used to measure the performance of R_s compensation. With a fixed-conductance model membrane, the amplifier bandwidth is normally determined by measuring the capacity transient decay time in response to a voltage step. However, with commercial amplifiers that incorporate standard R_s compensation, the

whole-cell charging current is delivered by an injection capacitor to avoid saturation before standard R_s compensation is applied (Sigworth, 1983); therefore, the current transient in response to a voltage step no longer reflects of the amplifier's bandwidth. Similarly, with amplifiers that use prediction or supercharging R_s correction circuits to speed up the response to a voltage step, the capacity transient cannot be used as a measure of the system's bandwidth (see Theory; Fig. 5). For these reasons, we measured R_s compensation performance in response to a step conductance change.

To create a step conductance change, we built a low-noise SPST switch (see Materials and Methods). We could not use ordinary field effect transistor or mechanical relay switches: the charge injection of field effect transistor switches obscures the current transients, and most mechanical switches are noisy and the contacts bounce.

First, we tested the performance of the Axopatch 1D, using the circuit and low-noise SPST switch described in Fig. 6, *A* and *B*. Set at 80% R_s compensation, the response time of the Axopatch 1D was >100 μs. At higher R_s compensation settings, the amplifier exhibited oscillations due to the inherent instabilities described above (see Theory), and surprisingly, the response time of the Axopatch 1D never decreased below 90 μs. From our experiments on Na$^+$ currents (see below), if the amplifier response time
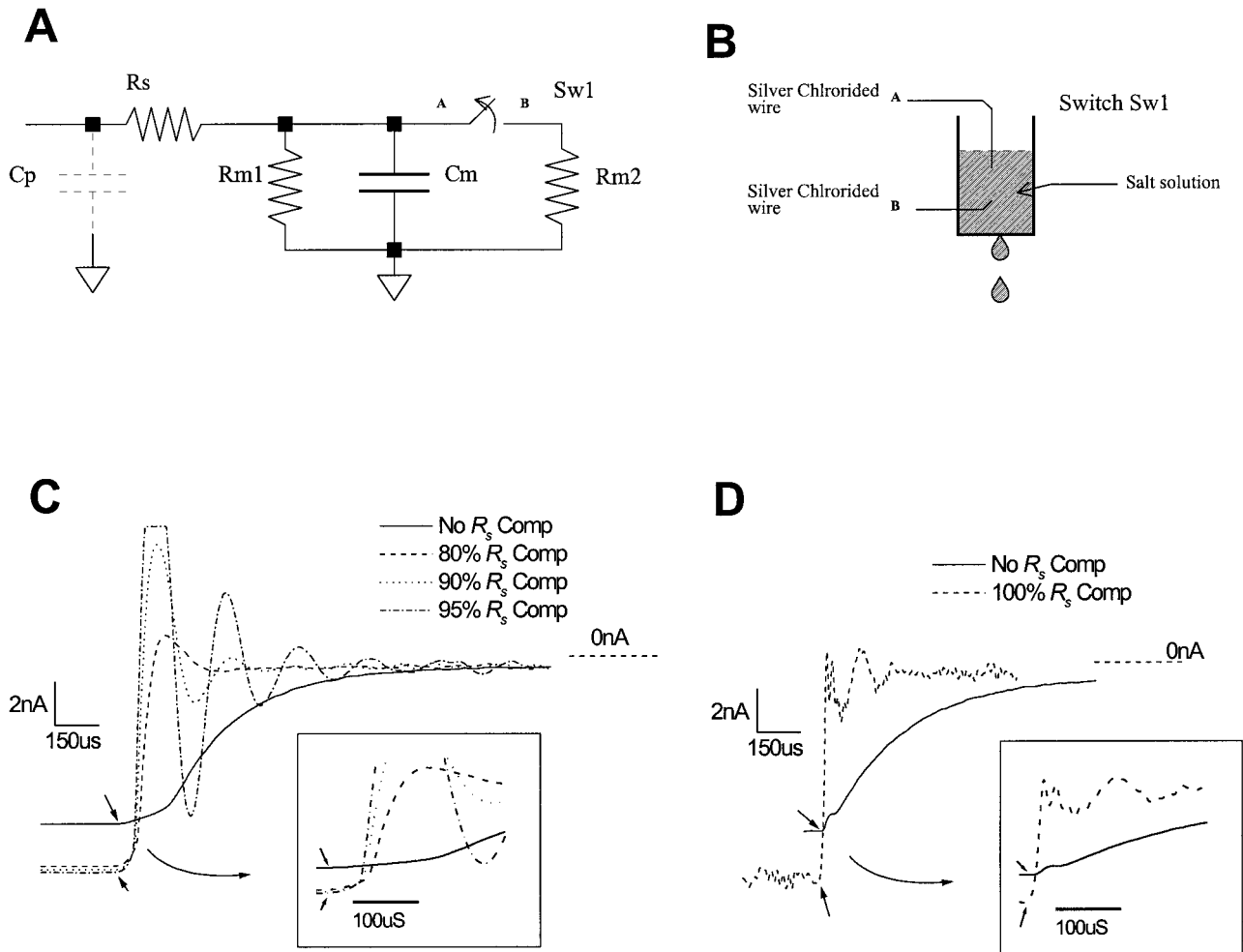
A

B

C

D

FIGURE 6 (*A*) Model circuit used for dynamic conductance change. (*B*) Low-noise, bounceless SPST switch implementation. When the tube is filled with solution, the switch is closed; as the fluid level drops below wire A, the switch opens. (*C, D*) Measured current response of Axopatch 1D, using standard R_s compensation. (*C*) Custom-built amplifier using state estimator R_s compensation (*D*) to step conductance change while holding at −100 mV. The switch Sw1 opening marked by arrow. R_s = 4.7 MΩ, C_p ≈ 1.5 pF, C_m = 47 pF, R_{m1} = 180 MΩ, R_{m2} = 10 MΩ. *Traces in C*: Low-pass filtered with a 4-pole Bessel filter at 10 kHz. *Traces in D*: Low-pass filtered with a 1-pole RC filter at 15 kHz.

is greater than 90 μs, one has difficulty measuring Na$^+$ currents from mammalian neurons under voltage-clamp conditions.

To ensure that the measured performance of the Axopatch 1D was not obscured by a switch artifact, we verified the performance of the SPST switch by setting R_s = 10 kΩ and using no R_s compensation. The recorded current trace showed a clean step transition in less than 20 μs with no measurable switch artifact (data not shown).

Next we repeated the test, using our amplifier. We adjusted for full R_s compensation by minimizing the capacity current transient decay time in response to voltage steps (see Materials and Methods). In contrast to what we observed for the Axopatch 1D, our amplifier responded in under 50 μs to a step conductance change, confirming the bandwidth and stability of state estimator R_s compensation predicted from the theory (Fig. 6 *D*). These results clearly demonstrate the advantages of using a state estimator to compensate for R_s.

Measurements of voltage-gated Na$^+$ currents

To demonstrate further the utility of state estimator R_s compensation when recording whole-cell currents with a single-electrode voltage clamp, we used our amplifier to measure ionic currents from single cells. As a stringent test, we measured voltage-gated inward Na$^+$ currents from nerve and muscle cells. Because these Na$^+$ currents are large and activate extremely rapidly, they are difficult to measure accurately with conventional single-electrode patch-clamp amplifiers (Schofield and Ikeda, 1988; Nerbonne and Gurney, 1989; Hanck, 1995; Sakakibara et al., 1993).

Rat SCG neurons

For our first experiments, we used cultured neonatal rat SCG neurons. We chose this preparation because voltage-gated Na$^+$ currents from adult rat SCG neurons have been

measured previously by two-electrode voltage-clamp techniques (Belluzzi and Sacchi, 1986), providing a reference for our measurements. In addition, these large neurons are difficult to voltage clamp with conventional single-electrode patch-clamp amplifiers (Schofield and Ikeda, 1988; Nerbonne and Gurney, 1989).

Fig. 7 A shows the membrane currents from a neonatal SCG neuron evoked by depolarizing voltage steps from a holding potential of -90 mV with no R_s compensation. Under these conditions the voltage-clamp bandwidth was too low to control V_m: with steps to -50 mV and greater, we observed a clear delayed inflection in the current records. These delayed inflections indicate loss of voltage control and the generation of unclamped action potentials. With further depolarization, the latency to evoke these unclamped action potentials decreased. The peak I-V curve for these currents (Fig. 7 A, *right*) has a corresponding discon-

tinuity at -50 mV, clearly deviating from the expected Hodgkin-Huxley (HH) description of Na^+ currents.

Fig. 7 B shows membrane currents and the corresponding peak I-V curves from the same neuron with full R_s compensation. With full R_s compensation, the bandwidth of the voltage-clamp amplifier is increased to $\sim$10 kHz, as predicted from the theory, and as indicated by the decay time of the capacity transients in response to voltage steps. In response to incrementing depolarizing voltage steps, we observed Na^+ currents that activated immediately at the end of the capacity transient and whose activation kinetics increased with increasing command voltages, as predicted from an HH description of voltage-gated Na^+ currents. In this neuron, with full R_s compensation, we did not observe delayed inflections in the current records and the generation of unclamped action potentials. The amplitude of the inward Na^+ current increased with successive depolarizations up to
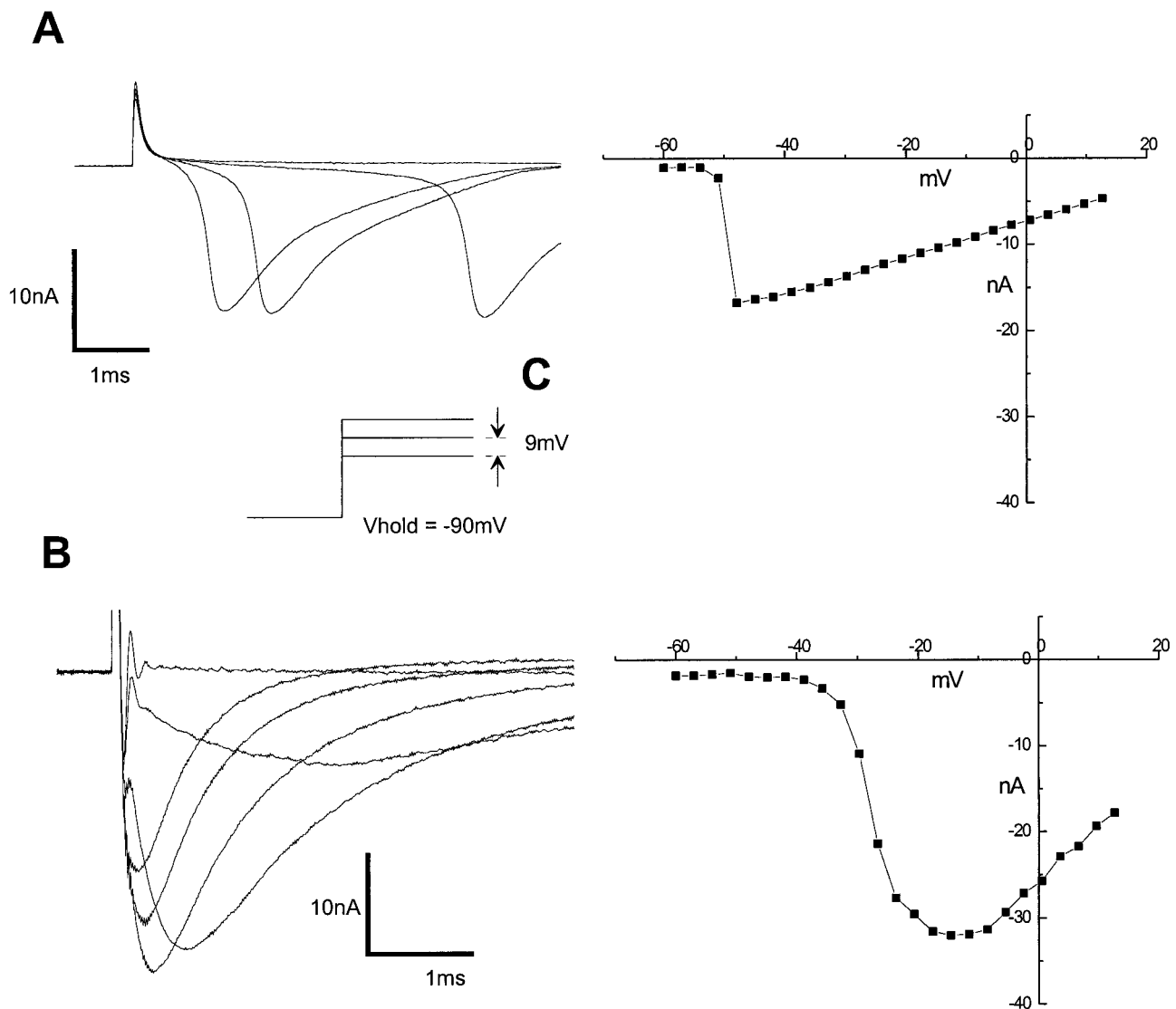

FIGURE 7 Voltage-clamped Na^+ current from a P1 SCG neuron in culture for 6 days ($C_m = 25$ pF; $R_s = 6$ MΩ). (*A, B*) Na^+ current activation and peak I-V curve using 0% and 100% R_s compensation, respectively. (*C*) Stimulation protocol for displayed traces in *A* and *C*.

−18 mV, reaching a maximum of 32 nA. The *I-V* curve shows that Na$^+$ current activation is a steep and continuous function of V_m (Fig. 7 *B*), similar to that obtained using two-electrode voltage-clamp studies of these neurons (Belluzzi and Sacchi, 1986).

Our ability to measure Na$^+$ currents depended critically on fully compensating for R_s. Fig. 8 shows our results from another neuron, with 100% and 80% R_s compensation. With 80% R_s compensation (Fig. 8 *A*) the control of V_m was improved because of the increased bandwidth, but it was still not sufficient to prevent the escape of V_m when the command voltage was stepped to −50 mV. At −50 mV, the Na$^+$ currents activated slowly with no detectable latency, as was the case with full R_s compensation; however, after ∼1 ms, we observed a clear inflection in the current, indicating the presence of an unclamped action potential. The insufficient bandwidth at 80% R_s compensation was readily ap-

parent from the corresponding *I-V* curve (Fig. 8 *A, right*); the *I-V* curve has a clear discontinuity starting at −50 mV, and compared to full R_s compensation in Fig. 8 *B*, the peak inward current was shifted leftward by ∼20 mV.

In practice, full R_s compensation was straightforward to achieve for the majority of the 31 neurons we studied. In 25 neurons (70%), we could successfully measure Na$^+$ currents under voltage-clamp conditions, similar to those shown in Fig. 7 *B*. In the remaining six cells we were unable to maintain voltage control, even though R_s compensation reduced the transient decay time to <70 μs. In these cells, the membrane resealed spontaneously, and the uncompensated capacity transient often had a multiexponential time course. While these cells usually had high (∼8–10 MΩ) access resistances, we were able to voltage clamp other neurons with equally high access resistance without difficulty. We suggest that the loss of voltage control arose from
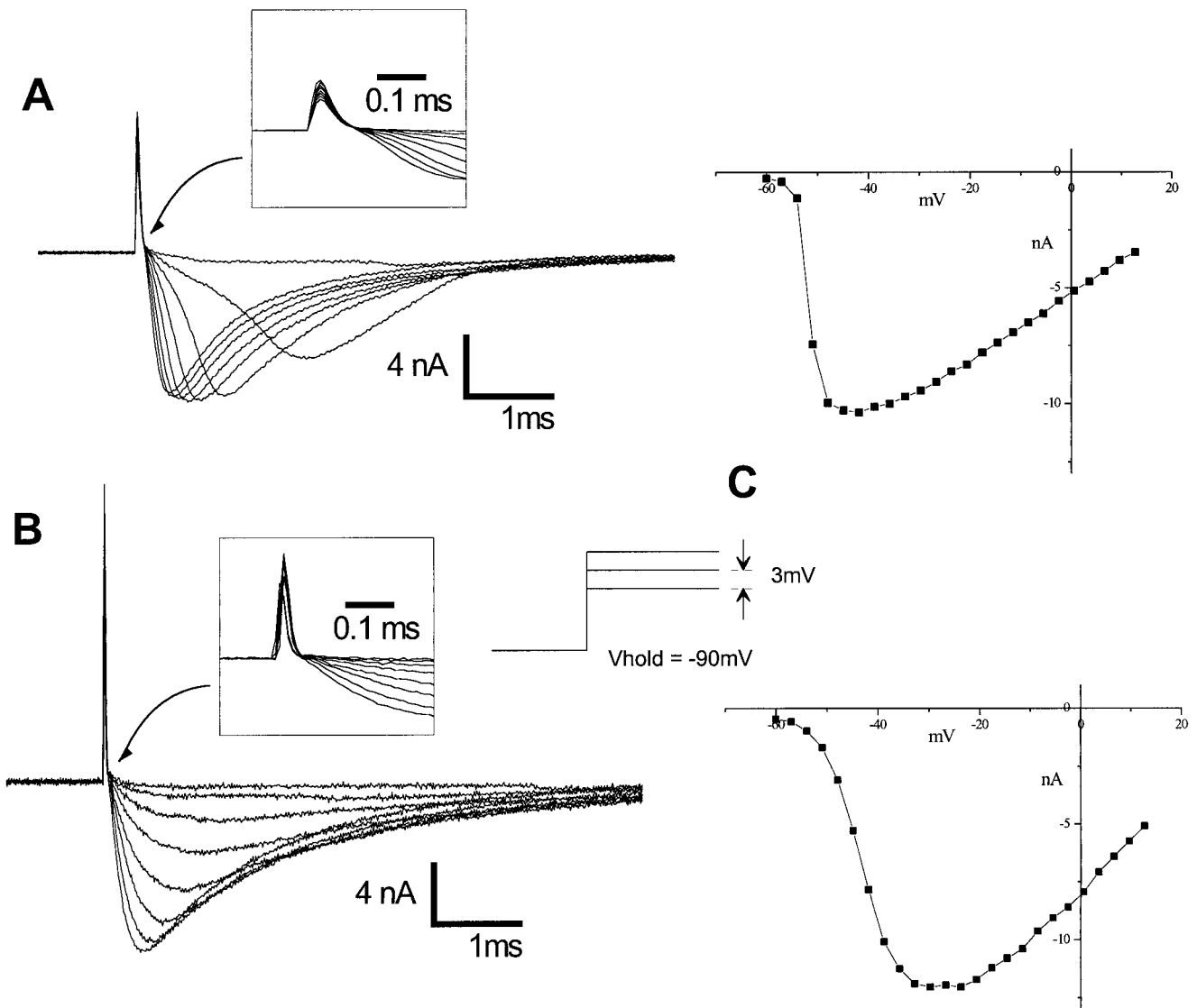

FIGURE 8   Voltage-clamped Na$^+$ current from a P1 SCG neuron in culture for 1 day (C_m = 12 pF; R_s = 5 MΩ). (*A, B*) Na$^+$ current activation and peak *I-V* curve using 80% and 100% R_s compensation, respectively. (*C*) Stimulation protocol for displayed traces in *A* and *C*.

incomplete membrane rupture, which added a series resistance with a more complicated equivalent circuit that could not be fully compensated for with state estimator R_s compensation.

Effective R_s using state estimator R_s compensation

Comparing Fig. 4 *A* with Eq. 5, it can be seen that full R_s compensation is achieved when R_{sest} is set equal to R_s. Even when this is so, there is still an effective R_s remaining. This is analogous to what occurs with a two-electrode voltage clamp, where the effective R_s is proportional to the R_s of the current injection electrode attenuated by the open-loop gain: as the open-loop gain is increased, the effective R_s decreases but never entirely vanishes. To measure the effective R_s achieved in practice, we adjusted the amplifier for full R_s compensation (see Materials and Methods) and then measured two successive peak *I-V* curves: curve 1 with a holding potential of -90 mV to remove Na^+ channel inactivation completely, and curve 2 with a holding potential of $\sim$ -70 mV to inactivate roughly half of the cell's Na^+ channels (Fig. 9). The effective R_s can then be estimated by comparing the points at which half-maximum inward current (half-maximum inward current) occurs in curves 1 and 2; given that half-maximum inward current occurs in curves 1 and 2 at points (V1, I1) and (V2, I2), respectively, the effective R_s is given by (V1 − V2)/(I1 − I2). For the cell shown in Fig. 9, the effective R_s was $\sim$220 kΩ, whereas the uncompensated R_s was 6 MΩ. In practice, the effective R_s ranged from 50 to 250 kΩ ($n = 5$).

In addition to neurons, we used our amplifier to measure voltage-gated Na^+ currents from isolated adult human heart ventricular myocytes. With full R_s compensation, the Na^+ currents activated immediately after the capacity transient (data not shown). The Na^+ currents peak amplitudes increased with successive depolarization up to -26 mV, reaching a maximum of 81.8 nA; there were no unclamped

action potentials or delayed inflections in the currents record. The *I-V* curve shows steep activation with V_m and no discontinuities.

CONCLUSION

In this paper, we demonstrate an improved method for compensating for R_s when recording in whole-cell patch-clamp configurations. This method is straightforward to implement, and amplifiers incorporating state estimator R_s compensation are extremely stable. The main aspect of this R_s compensation method is to compute V_m using a state estimator and to use this value in a feedback loop to implement a voltage clamp.

Using a model cell with parameter values representative of whole-cell recording, our benchtop tests show that state estimator R_s compensation responds to step conductance changes in well under 50 μs, whereas standard R_s compensation reaches a limit of $\sim$90 μs before the onset of oscillations. Our experiments on neurons demonstrate that it is essential to have such a rapid response to voltage clamp Na^+ currents reliably. Equally important, our experiments demonstrate that state estimator R_s compensation amplifiers perform well in actual physiological experiments. As such, these amplifiers should make it easier to measure large rapid ionic currents by whole-cell patch-clamp techniques.

APPENDIX: STABILITY ANALYSIS

This appendix compares the stability of various forms of R_s compensation with state estimator R_s compensation. First we analyze the stability of standard R_s compensation. We extend this analysis to include known modifications that improve stability: low-pass filtering of the R_s compensation signal, and the steady-state R_s compensation outlined by Moore et al. (1984) and Strickholm (1995b). Then the analysis is extended further to include state estimator R_s compensation, demonstrating quantitatively its improved stability over conventional approaches. Finally, we discuss configuration aspects that affect the stability of state estimator R_s compensation.

For each system an *s*-domain transfer function representation is given, which includes a feedback loop. The stability of the loop is determined by forming a Bode plot of the open-loop frequency response and applying the Nyquist stability criteria to determine the gain and phase margins.

Standard R_s compensation

Fig. A1 *A* shows a transfer function representation of standard R_s compensation similar to the one used by Sigworth (1983), but including the effects of pipette capacitance C_p (compare Fig. A1 *A* with Fig. 1). Block 1 gives the transfer function of I_p to V_p when $R_m \gg R_s$. Block 2 forms the R_s compensation signal V_{cor} by measuring I_p with a bandwidth set by τ_z and scaling it by αR_s (100% R_s compensation occurs when $\alpha \to 1$). The block diagram assumes that V_p is clamped using a feedback loop with much higher bandwidth than the R_s compensation feedback loop, as is the case using an *I-V* converter headstage, allowing interaction between each loop to be ignored (Sigworth, 1983). The open-loop transfer function of the
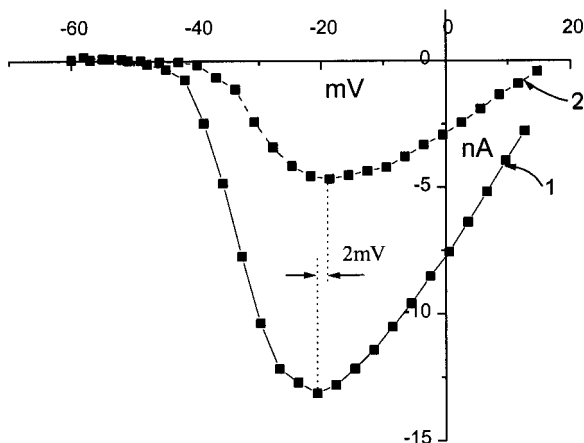
FIGURE 9   Measuring the effective R_s using state estimator R_s compensation. Peak *I-V* curves of Na^+ current activation from a SCG neuron in response to depolarizing voltage steps with $V_h = -90$ mV (*curve 1*, ——) and $V_h = -70$ mV (*curve 2*, − − −). $R_s = 6$ MΩ, effective $R_s = 220$ kΩ.

A
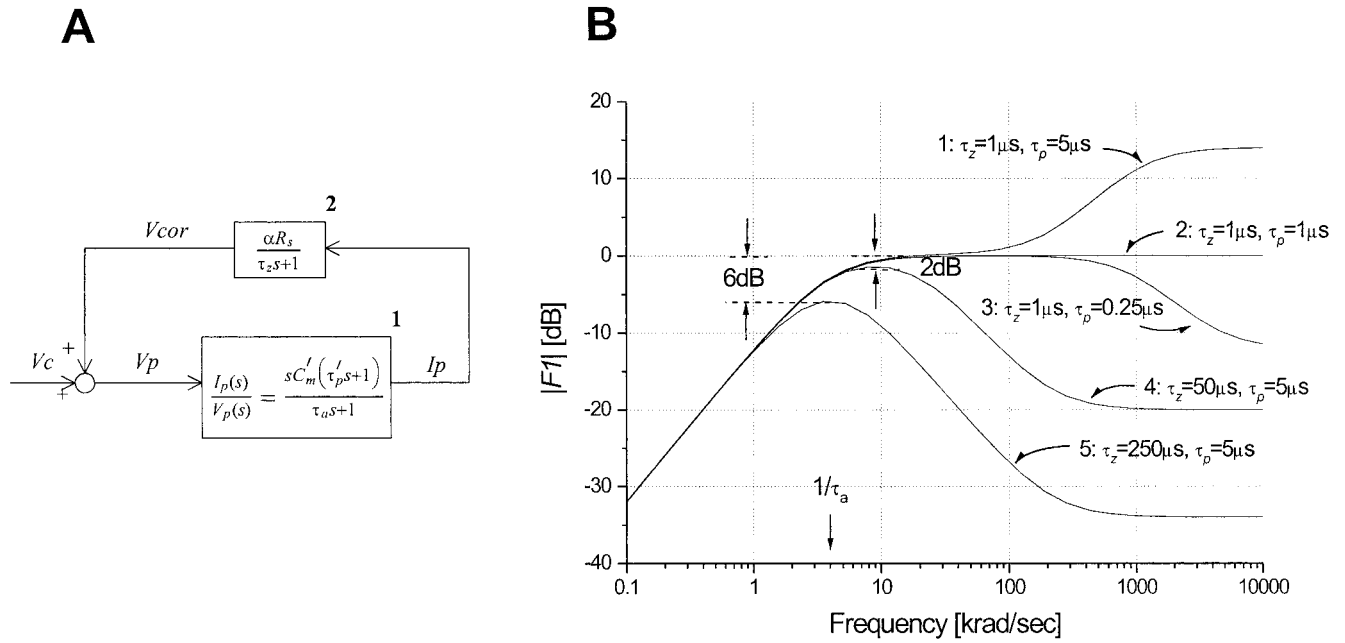   **B**

FIGURE A1   Stability of standard R_s compensation. (*A*) s-domain block. (*B*) Open-loop Bode plot of $|F_1(j\omega)|$. $R_s = 5$ MΩ, $C_m = 50$ pF, $\alpha = 1$, τ_p, τ_z as indicated.

feedback loop in Fig. A1 *A* is given by

$$F_1(s) = \frac{V_{cor}(s)}{V_c(s)} = \underbrace{\frac{sC_m'(\tau_p's + 1)}{(\tau_a s + 1)}}_{\frac{I_p}{V_p}} \times \underbrace{\frac{\alpha R_s}{(\tau_z s + 1)}}_{R_{scor}}$$

$$= \frac{\alpha \tau_a' s(\tau_p's + 1)}{(\tau_a s + 1)(\tau_z s + 1)} \qquad ((A1))$$

where

$$C_m' = (C_m + C_p) \cong C_m,$$

$$\tau_a' = R_s C_m' \cong \tau_a = R_s C_m,$$

$$\tau_p' = R_s \frac{C_m C_p}{C_m + C_p} \cong \tau_p$$

when $C_m \gg C_p$. To ensure stability, $|F_1(j\omega)| < 1$ when $\angle F_1(j\omega) \le 0$, which occurs when the slope of $|F_1(j\omega)| \le 0$. Fig. A1 *B* plots $|F_1(j\omega)|$ for various values of τ_z and τ_p so that the stability criteria can be verified.

In Fig. A1 *B*, traces 1–3 illustrate wideband R_s compensation ($\tau_z = 1$ μs) with decreasing pipette capacitance. For these three traces, when $\omega < 1/\tau_a$ $|F_1(j\omega)|$ is dominated by the zero at the origin, rising at 20 dB per decade with a 90° phase angle so that the stability criteria are not violated. When $1/\tau_a < \omega < 1/\tau_p$, $F_1(s)$ is dominated by the pole at $-1/\tau_a$ and the zero at the origin such that $\angle F_1(j\omega) \to 0$, and $|F_1(j\omega)| \to 1$ when $\alpha \to 1$. Consequently, the gain margin $\to 0$, which predicts that the system will be unstable. Marginal stability is achieved by decreasing α so that $|F_1(j\omega)|$ remains less than unity; stable performance requires $\alpha \approx 0.8$, but this causes the voltage clamp bandwidth to be reduced to ~3 kHz ($\tau_a = 0.2 *$ 5 MΩ * 50 pF). When $\omega > 1/\tau_z$, $1/\tau_p$ $F_1(s)$ is dominated by the pole at $-1/\tau_z$ and the zero at $-1/\tau_p$. Therefore, if $\tau_p > \tau_z$, $|F_1(j\omega)| > 1$ at high frequencies, which predicts that the system will be unstable (*trace 1*). To ensure stability $\tau_p \le \tau_z$, so that $|F_1(j\omega)|$ remains less than unity (*traces 2 and 3*). This is achieved by using pipette capacitance neutralization to reduce the effective C_p, thus lowering τ_p. In practice, the effectiveness of

capacitance neutralization is compromised at higher frequencies, and so τ_p must be reduced to considerably less than τ_z (*trace 3*) (Sigworth, 1983) .

Stabilizing standard R_s compensation: low-pass filtering the R_s compensation signal

Standard R_s compensation can be stabilized by lowering the bandwidth of the R_s compensation signal by increasing τ_z. As shown in traces 4 and 5 of Fig. 10 *A*, increasing τ_z increases the gain margin, thereby increasing stability. However, this stability is achieved at the expense of lowering the voltage clamp bandwidth of V_m. When τ_z is increased to τ_a (*trace 5*), the gain margin is increased to ~6 dB, but the resultant voltage-clamp bandwidth in this case is only ~600 Hz. Trace 4 shows a compromise when $\tau_z = 50$ μs. This corresponds to the strategy employed by voltage clamps such as the Axopatch 200 series (Axon Instruments), where the "lag" control adjusts a time constant analogous to τ_z that ranges from 5 to 100 μs. As shown, setting $\tau_z = 50$ μs gives an extra ~2 dB of gain margin, allowing somewhat higher α settings to be used before the onset of instability, with a voltage clamp bandwidth of ~2 kHz. This type of filtering becomes more effective in increasing stability when τ_a is small (low R_s and/or low C_m), because the corner frequency at $1/\tau_a$ moves closer to $1/\tau_z$, keeping $|F_1(j\omega)|$ further below the 0 dB axis. Even then, it is not possible to increase the gain margin by more than ~5 dB, which is insufficient for good stability.

Stabilizing standard R_s compensation: steady-state R_s compensation

Figure A2 shows a block diagram of standard R_s compensation incorporating a bridge to subtract the membrane capacity current, as described by Strickholm (1995a). Block 1 gives the transfer function of I_p to V_p, ignoring the effects of C_p. Block 2 forms the R_s correction signal as in Fig. 10 *A*, and block 3 and summing node S1 implement the bridge subtraction.
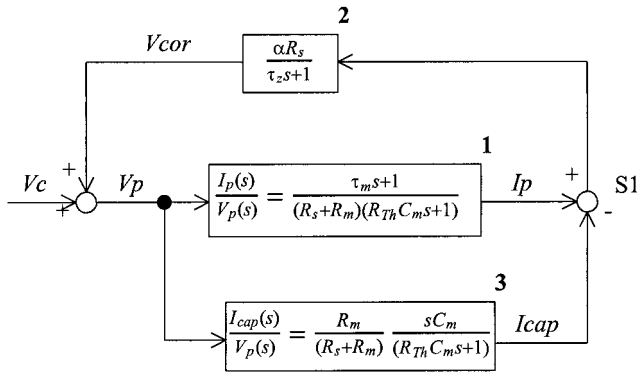
FIGURE A2   s-domain block diagram of steady-state R_s compensation.

Solving for the open-loop transfer function of Fig. A2 gives

$$F_2(s) = \frac{V_{corr}(s)}{V_c(s)} = \frac{\alpha R_s}{(R_s + R_m)(R_{Th}C_m s + 1)(\tau_z s + 1)}$$

$$= \underbrace{\frac{\tau_m s + 1}{(R_s + R_m)(R_{Th}C_m s + 1)}}_{\frac{I_p}{V_p}} \times \underbrace{\frac{\alpha R_s}{\tau_z s + 1}}_{R_{scorr}} \times \frac{1}{\tau_m s + 1} \quad (A2)$$

where

$$R_{Th} = \frac{R_s R_m}{R_s + R_m} \cong R_s \quad \text{when } R_m \gg R_s.$$

Equation A2 shows that for the purposes of calculating stability, the bridge subtraction acts like a low-pass filter with time constant $\tau_m = R_m C_m$ that filters the R_s compensation signal (see Moore et al. (1984) for a similar derivation). Therefore, steady-state R_s compensation increases stability in the same manner as would be achieved by setting $\tau_z = \tau_m$ using standard

R_s compensation, as outlined above. The consequent reduction of voltage clamping bandwidth using steady-state R_s compensation is illustrated in Fig. 5 A.

State estimator R_s compensation

To extend the stability analysis to cover state estimator R_s compensation, it is necessary to model the interaction between the voltage-clamp feedback loop and the R_s compensation feedback loop. This is done in Fig. A3 A, where the voltage-clamp feedback loop is included in the block diagram. Note that as $E \to \infty$ in Fig. A3 A, the transfer function of the voltage-clamp feedback loop can be replaced by a constant, and the block diagram reduces to that shown in Fig. A1 A. Fig. A3 B shows the equivalent block diagram after algebraic manipulation. Solving for the open loop transfer function of Fig. A3 B gives

$$F_3(s) = \frac{V_{fbk}(s)}{V_c(s)} \qquad (A3)$$

$$= E\left[\frac{(\tau_a \tau_z - \alpha \tau_a \tau_p)s^2 + (\tau_a - \alpha \tau_a + \tau_z - \alpha \tau_p)s + 1}{(\tau_a s + 1)(\tau_z s + 1)}\right]$$

The important fact to notice about Eq. A3 is that when $\alpha \to 1$ (full R_s compensation) and $\tau_z \to \tau_p$, the numerator of the bracketed term of Eq. A3 goes to unity, giving

$$F_4(s) = E\left[\underbrace{\frac{1}{\tau_a s + 1}}_{\frac{V_m}{V_c}} \frac{1}{\tau_z s + 1}\right] \qquad (A4)$$

As indicated, V_{fbk} is then equivalent to a direct measurement of the membrane voltage V_m filtered by a one-pole filter with time constant τ_z. Alternatively, note that when $\alpha \to 1$ and $\tau_z \to \tau_p$, Fig. A3 B satisfies the estimator equation (Eq. 5), as can be shown directly by dividing both sides of Eq. 5 by $(\tau_p s + 1)$ and noting that V_{fbk} then equals $V_m/(\tau_p s + 1)$. When the estimator equation is satisfied, the voltage clamp of Fig. A3 B has greatly enhanced stability, as shown in Fig. A3 C. For stable operation
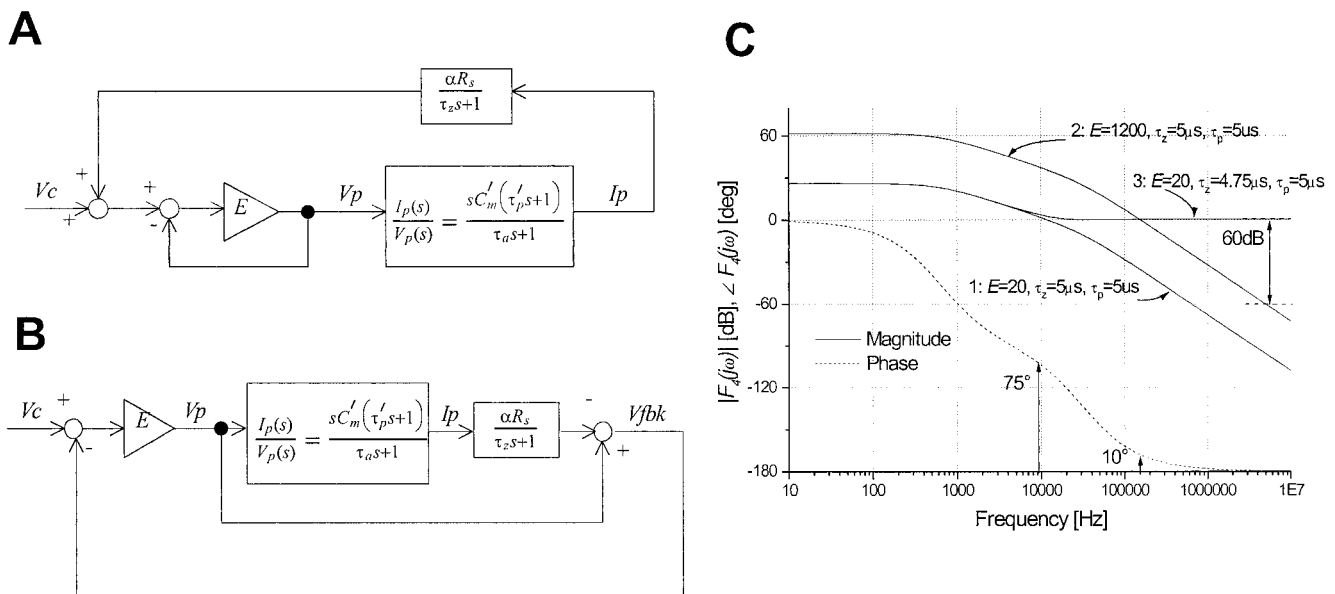

FIGURE A3   Stability of state estimator R_s compensation. The state estimator equation is satisfied when $\alpha = 1$ and $\tau_z = \tau_p$. (A, B) s-domain block diagram showing voltage-clamp feedback loop with gain E. (C) Open-loop Bode plot of $|F_4(j\omega)|$ and $\angle F_4 (j\omega)$. $R_s = 5$ MΩ, $C_m = 50$ pF, $\alpha = 1$, E, τ_p, and τ_z as indicated.

$|F_4(j\omega)| < 1$ when $\angle\; F_4(j\omega) \leq 180°$, which occurs when the slope of $|F_4(j\omega)|$ approaches -40 dB/decade. Trace 1 of Fig. A3 C plots $|F_4(j\omega)|$ when $E = 20$, showing a gain margin of 60 dB and a phase margin of $75°$, predicting excellent stability. In addition, when the estimator equation is satisfied, the 0-dB cross-over frequency (f_{co}) indicates the closed-loop voltage clamp bandwidth of V_m, which is $\sim$10 kHz. Thus the voltage clamp of Fig. A3 B has 100% R_s compensation, wide stability margins, and a voltage clamp bandwidth of 10 kHz. In contrast, the voltage clamp using standard R_s compensation and an I-V converter headstage, with the same pipette and cell parameters, has narrow stability margins and a voltage clamp bandwidth of 3 kHz (see *trace 4*, Fig. A1 B). (In practice, a gain of 20 is too low to maintain adequate steady-state accuracy. This can be rectified by replacing the gain block E with a controller that has a higher DC gain (see, for example, the "pole zero" compensation discussed by Horowitz and Hill (1989)). For reasons discussed below, our voltage clamp uses a current source in the headstage that has the added benefit of solving the low DC gain problem.)

If E is increased beyond $\sim$1000 (*trace 2*, Fig. A3 C), $|F_4(j\omega)|$ crosses the 0 dB axis with a slope approaching -40 dB/decade because of the effects of the second pole at $-1/\tau_z$, predicting unstable operation. This explains why no stability advantage is conferred, even if the estimator equation is satisfied when a traditional I-V converter headstage is used, because an I-V converter headstage is equivalent to Fig. A3 B with a very large ($>$100,000) E.

The wide stability margins conferred using state estimator R_s compensation are dependent on the cancellation of terms in the numerator of Eq. A3, which requires that τ_z be adjusted so as to match τ_p. Consequently, mismatches of τ_z in relation to τ_p lead to incomplete cancellation and unstable operation. This effect is shown in trace 3 of Fig. A3 C, where the mismatch of τ_z reduces the gain margin to zero. Fortunately, the matched state coincides with maximum stability and maximum bandwidth at full R_s compensation, facilitating adjustment. This contrasts with standard R_s compensation, which is unstable at full R_s compensation and high bandwidth, regardless of any adjustments of τ_z.

Implementing estimator R_s compensation: low-impedance versus high-impedance headstage

To achieve high stability when the estimator equation is satisfied, it is important for the measured values of I_p and V_p to be accurate up to $\sim$1 decade above f_{co}. Otherwise, phase mismatch introduces two real left-hand plane zeros in Eq. A3 due to incomplete cancellation of terms in the numerator; this lowers gain margin and decreases stability. In practice it is easier to satisfy this requirement when the headstage presents a high impedance to the pipette at high frequencies. If the headstage presents a low impedance, the pipette capacitance C_p draws a large current at high frequencies, which is difficult to measure accurately; a high impedance limits this current. A voltage clamp with a high-impedance headstage is modeled in Fig. A4, where a controlled current source (CCS) presents a high (ideally infinite) impedance to the pipette. In Fig. A4, block 1 represents an ideal CCS with transconductance G_0. Block 2 gives the transfer function of V_p to I_p when $R_m \gg R_s$, and block 3 forms the R_s
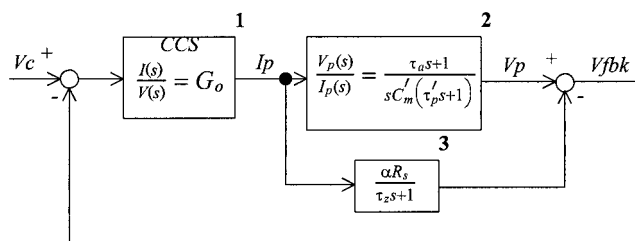
compensation signal as in Fig. 10. Solving for the open-loop transfer function of Fig. A4 gives

$$F_5(s) = \frac{V_{fbk}(s)}{V_c(s)}$$

$$= G_0\left[\frac{(\tau_a\tau_z - \alpha\tau_a\tau_p)s^2 + (\tau_a - \alpha\tau_a + \tau_z - \alpha\tau_p)s + 1}{sC'_m(\tau'_p s + 1)(\tau_z s + 1)}\right]$$

(A5)

Note that the numerator in brackets of Eq. A5 is the same as that in Eq. A3, so that Eq. A5 becomes

$$F_6(s) = G_0\left[\underbrace{\frac{1}{sC'_m(\tau'_p s + 1)}}_{\frac{V_m}{I_p}}\;\frac{1}{\tau_z s + 1}\right]\text{ when }\alpha \to 1, \tau_z \to \tau_p$$

(A6)

and V_{fbk} is then equivalent to a direct measurement of the membrane voltage V_m, filtered by a one-pole filter with time constant τ_z. Similar to Fig. A3 B, when $\alpha \to 1$ and $\tau_z \to \tau_p$, Fig. A4 satisfies the estimator equation (Eq. 5), and the voltage clamp has greatly enhanced stability (see Fig. 4, B and C). An added benefit of using a CCS is the high DC gain due to the pole at the origin of Eq. A6, limiting steady-state error.

REFERENCES

Belluzzi, O., and O. Sacchi. 1986. A quantitative description of the sodium current in the rat sympathetic neurone. *J. Physiol. (Lond.).* 380:275–291.

Brennecke, R., and B. Lindemann. 1972. Theory of a membrane voltage clamp with discontinuous feedback through a pulse current clamp. *Rev. Sci. Instrum.* 45:184–188.

Finkel, A. S., and S. J. Redman. 1984. Theory and operation of a single microelectrode voltage clamp. *J. Neurosci. Methods.* 11:101–127.

Hanck, D. A. 1995. Biophysics of sodium channels. *In* Cardiac Electrophysiology. From Cell to Bedside. D. P. Zipes and J. Jalife, editors. W. B. Saunders Company, New York. 65–74.

Horowitz, P., and W. Hill. 1989. The Art of Electronics, 2nd Ed. Cambridge University Press, London.

McFarlane, S., and E. Cooper. 1992. Postnatal development of voltage-gated K currents on rat sympathetic neurons. *J. Neurophysiol.* 67: 1291–1300.

Moore, J. W., M. Hines, and E. M. Harris. 1984. Compensation for resistance in series with excitable membranes. *Biophys. J.* 46:507–514.

Nerbonne, J. M., and A. M. Gurney. 1989. Development of excitable membrane properties in mammalian sympathetic neurons. *J. Neurosci.* 9:3272–3286.

Sakakibara, Y., T. Furukawa, D. H. Singer, H. Jia, C. L. Backer, C. E. Arentzen, and J. A. Wasserstrom. 1993. Sodium current in isolated human ventricular myocytes. *Am. J. Physiol.* 265:H1301–H1309.

Schofield, G. G., and S. R. Ikeda. 1988. Sodium and calcium currents of acutely isolated adult rat superior cervical ganglion neurons. *Pflugers Arch.* 411:481–490.

Sigworth, F. J. 1983. Electronic design of the patch clamp. *In* Single-Channel Recording. B. Sakmann and E. Neher, editors. Plenum Press, New York. 3–35.

Strickholm, A. 1995a. A supercharger for single electrode voltage and current clamping. *J. Neurosci. Methods.* 61:47–52.

Strickholm, A. 1995b. A single electrode voltage, current and patch-clamp amplifier with complete stable series resistance compensation. *J. Neurosci. Methods.* 61:53–66.

Wilson, W. A., and M. M. Goldner. 1975. Voltage clamping with a single microelectrode. *J. Neurobiol.* 6:411–422.

FIGURE A4 s-domain block diagram of voltage clamp, using a controlled current source (CCS) with state estimator R_s compensation.